Dalton Transactions

PAPER

Cite this: *Dalton Trans.*, 2017, **46**, 3400

Synthesis, structural characterization and magnetic behaviour of a family of $[Co^{III}_2Ln^{III}_2]$ butterfly compounds†

Alejandro V. Funes,[a] Luca Carrella,[b] Yvonne Rechkemmer,[c] Joris van Slageren,[c] Eva Rentschler[b] and Pablo Alborés*[a]

Received 13th December 2016,
Accepted 16th February 2017

DOI: 10.1039/c6dt04713k

rsc.li/dalton

We have successfully prepared and structurally characterized a family of butterfly-like $[Co^{III}_2Ln^{III}_2]$ complexes where all magnetic properties are due to the Ln(III) ions. The complexes with Ln = Tb(**1**), Dy(**2**), Ho(**3**), Er(**4**) and Yb(**5**) are iso-structural. An exception is the complex with Ln = Gd(**6**) which strings in a one dimensional chain. The structural similarity together with the high tendency of the crystallites to align under an applied magnetic field allowed an overall DC magnetic data treatment to extract phenomenological crystal field parameters and hence to determine the ground state multiplet energy level splitting. The Dy(III) member is the only one showing slow relaxation of magnetization under zero DC applied field, while all the others need a small DC applied field.

Introduction

The research field of molecular magnetism has been continuously increasing during the last few decades as Single Molecule Magnets (SMMs) show a promising avenue towards a variety of potential applications. SMMs could be used for high-density information storage,[1] magnetic refrigerants[2] or even play a crucial role in molecular spintronics.[3] Single molecule magnets exhibit slow relaxation of magnetization and hence potential bistability of exclusive molecular origin.[4] The main requisite for a compound showing SMM properties is that of possessing a large magnetic anisotropy, while a large S value has been proven not to be required.[5] In this context, research interest in the field has opened from a predominant study of polymetallic systems towards the study of low nuclearity, including single ion systems.

Regarding the type of metal involved, during the last few decades, main attention has been focused on the synthesis of homo- and heterometallic 3d complexes with SMM behaviour.[6] However more recently, it has been clearly demonstrated that the employment of highly anisotropic 4f ions can greatly enhance the SMM properties.[7] The use of anisotropic 4f ions for the design of improved SMMs can be classified into two different groups, single ion 4f and polynuclear 4f SMMs.[8] As a further development, combined 3d/4f systems are continuously being studied.[5b,9] Recent reports have shown that incorporation of 3d metals into pure 4f complexes may lead to drastic improvements in the SMM performance, mainly due to contributing to the suppression of quantum tunnelling pathways, responsible for the lack of hysteresis in most of the 4f based systems.[10]

In this context, a series of butterfly-like $[Co^{III}_2Dy^{III}_2]$ SMMs have been recently reported,[11] including our own contribution which became the first example within this series that shows two resolved relaxation pathways under zero DC external applied field.[12] Very recently a second example with two well resolved relaxation processes based on the acac ligand, $[Co^{III}_2Dy^{III}_2(OH)_2(teaH)_2(acac)_6]$,[11b] has also been reported, however in this case it seems that both relaxation processes are due to both crystallographically independent molecules in the unit cell. It is observed that very subtle changes in the coordination spheres of the metallic centres along this family of compounds provoke drastic changes in the magnetic behaviour, namely magnetization relaxation processes.

On the other hand, no examples of this type of $[Co^{III}_2Ln^{III}_2]$ compound have been reported where a family of Ln(III) ions has been explored in order to analyse the influence of Ln(III) over magnetic behaviour. Through an extension of our previous work on the $[Co^{III}_2Dy^{III}_2]$ system[12] we have been able to

[a]*Departamento de Química Inorgánica, Analítica y Química Física/INQUIMAE (CONICET), Facultad de Ciencias Exactas y Naturales Universidad de Buenos Aires, Pabellón 2, Ciudad Universitaria, C1428EHA Buenos Aires, Argentina. E-mail: albores@qi.fcen.uba.ar; Fax: +5411/4576-3341*

[b]*Institut für Anorganische Chemie und Analytische Chemie, Johannes Gutenberg - Universität Mainz, Duesbergweg 10-14, D-55128 Mainz, Germany*

[c]*Institut für Physikalische Chemie, Universität Stuttgart, Pfaffenwaldring 55, D-70569 Stuttgart, Germany*

†Electronic supplementary information (ESI) available. CCDC 1489634–1489638. For ESI and crystallographic data in CIF or other electronic format see DOI: 10.1039/c6dt04713k

prepare and structurally characterize a whole family of butterfly complexes with the Ln(III) ions from Gd to Yb (with the exception of Tm). $[Co^{III}_2Ln^{III}_2(OCH_3)_2(teaH)_2(Piv)_6]$, Piv = trimethylacetate, (Ln = Tb(**1**), Dy(**2**), Ho(**3**), Er(**4**) and Yb(**5**)) are isostructural complexes while the related complex $[Co^{III}_2Gd^{III}_2(OCH_3)_2(OHCH_3)_2(tea)_2(Piv)_4(HPiv)_2][Co^{III}_2Gd^{III}_2(OCH_3)_2(tea)_2(Piv)_4(HPiv)_2]_n$ (**6**) shows a polymeric structure. We are discussing here the magnetic behaviour of these new complexes mainly pointing out the existence or not of slow relaxation of magnetization.

Results and discussion

Synthesis and structural characterization

As we have shown in previous reports that the complex $Co_2(\mu\text{-}H_2O)(Piv)_4(HPiv)_4$ is an excellent precursor for building up molecular clusters including Co(II) and/or Co(III) ions,[12,13] we have explored its reaction with lanthanide ions, and in particular with nitrate hydrates, $Ln(NO_3)_3{\cdot}xH_2O$ in the presence of the versatile triethanolamine ($teaH_3$) ligand. The reaction was performed in acetonitrile with the addition of triethylamine as a base for aiding deprotonation of the $teaH_3$ ligand (Scheme 1). Blue crystals were obtained after a couple of weeks but, in most cases, not of suitable quality for X-ray structural determination. After re-crystallization from a mixture of methanol/acetonitrile solvent high quality single crystals were obtained for all used lanthanide ions. Structural characterization affords the formula: $[Co^{III}_2Ln^{III}_2(OCH_3)_2(teaH)_2(Piv)_6]$ with the exception of Ln = Gd which surprisingly results in a 1D polymeric arrangement: $[Co^{III}_2Gd^{III}_2(OCH_3)_2(OHCH_3)_2(tea)_2(Piv)_4(HPiv)_2][Co^{III}_2Gd^{III}_2(OCH_3)_2(teaH)_2(Piv)_6]_n$. This synthetic procedure proved robust with high reproducibility after several preparations, including the polymeric Gd compound.

In a previous communication we have already described the structure of the Dy member of this family,[12] which proves to be iso-structural with all other Ln(III) congeners reported here. The asymmetric unit of the triclinic $P\bar{1}$ cell consists of a half of the molecule which lies upon the crystal inversion centre, thus making both Ln(III) and Co(III) coordination spheres strictly equivalent. The metal ion core displays a butterfly like arrangement with wings at the opposite sides of the plane containing the body core. The Co(III) ions are at the outer 'wing' positions while the Ln(III) ions at the body sites. Each Ln(III) ion is coordinated *via* two μ_3-methoxide ligands, two μ_2-O atoms of the opposing doubly deprotonated $teaH^{2-}$ ligands, two μ_2-O atoms of also opposing pivalates and finally by both O atoms of a κ^2-capping pivalate (Fig. 1). The crystallographically unique Ln(III) ion is eight coordinate with a distorted SAP (square antiprism) geometry and Ln–O distances are in the range of 2.206(2) to 2.460(3) Å (see the ESI†). These values are in agreement with the values for all the other reported compounds bearing a $\{Co^{III}_2Ln^{III}_2\}$ butterfly like core (2.236–2.555 Å). Analysis of the coordination geometry, with SHAPE,[14] shows minimum Continuous Shape Measures (CShM's) for a SAP geometry with values of 1.919 (**1**), 1.889 (**2**), 1.910 (**3**), 1.918 (**4**) and 1.854 (**5**). The values of CShM between 0.1 and 3 usually correspond to a non-negligible but still small distortion from ideal geometry. It is clear that all these complexes span a narrow range of CShM's. This becomes a relevant point when discussing structural aspects of this family of complexes. However, it should be remarked at this point, that the real charge distribution of the Ln(III) coordination sphere has, in principle, nothing to do with this pure geometrical evaluation, as the different electron densities at each O atom must be considered. The Co(III) ions are in a six coordinate, octahedral environment, with Co–O bond distances ranging from 1.881(3)–1.936(2) Å and the Co–N bond distance ranging from 1.984(4)–1.991(4) Å, characteristic of the Co^{III} oxidation state (see the ESI†). Hydrogen bond interactions between the protonated O–H of the $teaH^{2-}$ ligands and

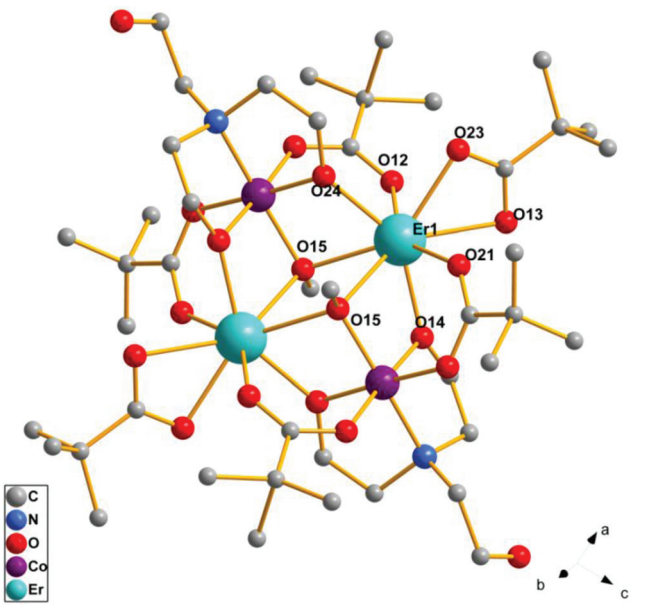

Fig. 1 Ball and sticks molecular representation of compound **4** structure. Hydrogen atoms have been omitted for the sake of clarity.

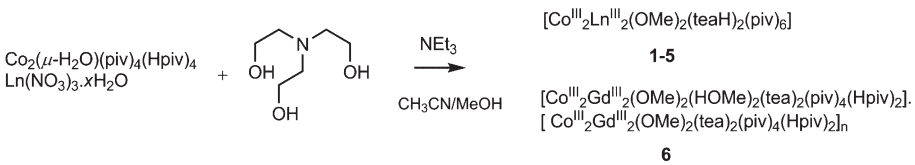

Scheme 1 Synthetic procedure for preparation of reported complexes.

the neighbouring molecule coordinated κ^2-pivalate ligand held molecules in chains running along the *c*-direction (see the ESI†). The shortest inter-molecular Ln···Ln distances between 8.290–8.360 Å within the family are twice larger than the intra-molecular Ln–Ln distances, ranging from 4.0408(4)–4.2017(6) Å along the series (see the ESI†). They are not explained in terms of H-interactions, but rather through the *tert*-butyl van der Waals interactions among chains. Ln···Ln distances along the chain direction are even larger, ranging from 12.142 to 12.209 Å for the different members of the series.

The gadolinium species crystallizes in a polymeric 1D structure, with a dimeric repeating unit consisting of $[Co^{III}_2Gd^{III}_2]$ moieties with alternated orientation of the Co–Co axis (Fig. 2). Notably, each moiety within this dimeric block retains the inversion center, making both Co(III) and Gd(III) of the same core symmetry-related. The Co–Co axis alternation (making an angle of *ca.* 55°) allows the polymerization through the tea^{3-} ligand pendant alkoxide arm. Compared to the non-polymeric structure, in both units of the dimeric block, the κ^2-capping pivalate is replaced by a κ^1-pivalate and a methanol molecule or the bridging O of the tea^{3-} pendant arm. This creates small differences in the Gd coordination sphere while the Co(III) environment remains the same as in the non-polymeric structure with just subtle metrics deviations (see the ESI†). Gd(III) still shows a SAP geometry but now with a CShM of 0.865/0.828. Gd–O bond distances span a similar range to the non-polymeric Ln(III) family members in both units of the dimeric block, 2.284(3)–2.530(3) Å (see the ESI†).

Chains run parallel to the *bc* plane making an angle of *ca* 32° with respect to the *c*-axis. They are well isolated due to the bulky *tert*-butyl groups of pivalate ligands while showing inter-chain H-bond interactions all along the *bc* plane (see the ESI†). The shortest Gd···Gd intra-chain distance is 9.698(1) Å while the shortest Gd···Gd inter-chain distance is 9.387(1) Å, both clearly longer than intra-molecular Gd–Gd distances of 4.2000(6)/4.2017(6) Å. This is an important feature when dealing with possible exchange or dipolar interactions.

Static magnetic properties

Direct current (DC) magnetic susceptibility measurements were performed on the single crystal crop of the complexes **1–6** in the 2–300 K temperature range and under an applied field of 1 kOe for two different situations: first without preventing the crystallite free movement under the applied magnetic field and thereafter with preventing orientation by silicone grease embedding. The room temperature $\chi_m T$ values of the restrained samples, 20.4 $cm^3\ mol^{-1}\ K$ (**1**), 29.1 $cm^3\ mol^{-1}\ K$ (**2**), 29.4 $cm^3\ mol^{-1}\ K$ (**3**), 21.8 $cm^3\ mol^{-1}\ K$ (**4**), 4.1 $cm^3\ mol^{-1}\ K$ (**5**) and 32.4 $cm^3\ mol^{-1}\ K$ (**6**), are close to the expected values for two non-interacting Ln(III) ions (four Gd(III) in the case of the repeating unit of **6**), 23.6 $cm^3\ mol^{-1}\ K$ (**1**), 28.3 $cm^3\ mol^{-1}\ K$ (**2**), 28.1 $cm^3\ mol^{-1}\ K$ (**3**), 22.9 $cm^3\ mol^{-1}\ K$ (**4**), 5.1 $cm^3\ mol^{-1}\ K$ (**5**) and 31.5 $cm^3\ mol^{-1}\ K$ (**6**), in spherical symmetry. Upon cooling, the $\chi_m T$ values fall gradually, down to 30–50 K depending on the different Ln(III), before plummeting close to 10–15 K to reach values of 11.9 $cm^3\ mol^{-1}\ K$ (**1**), 14.3 $cm^3\ mol^{-1}\ K$ (**2**), 15.4 $cm^3\ mol^{-1}\ K$ (**3**), 10.2 $cm^3\ mol^{-1}\ K$ (**4**), and 2.5 $cm^3\ mol^{-1}\ K$ (**5**) at 2 K (Fig. 3). This behaviour can be mostly attributed to the depopulation of the crystal field split m_J sublevels, with also a possible onset of weak antiferromagnetic exchange and/or dipolar interactions mainly contributing at very low *T*. In contrast, in the case of Gd compound **6**, the $\chi_m T$ value remains essentially constant up to 15 K when it abruptly increases to reach a final magnitude of 42.6 $cm^3\ mol^{-1}\ K$ at 2 K. This is the expected profile for the spin-only behaviour of the Gd(III) $^8S_{7/2}$ ($L = 0$, $S = 7/2$) ground state exhibiting weak ferromagnetic exchange interactions.

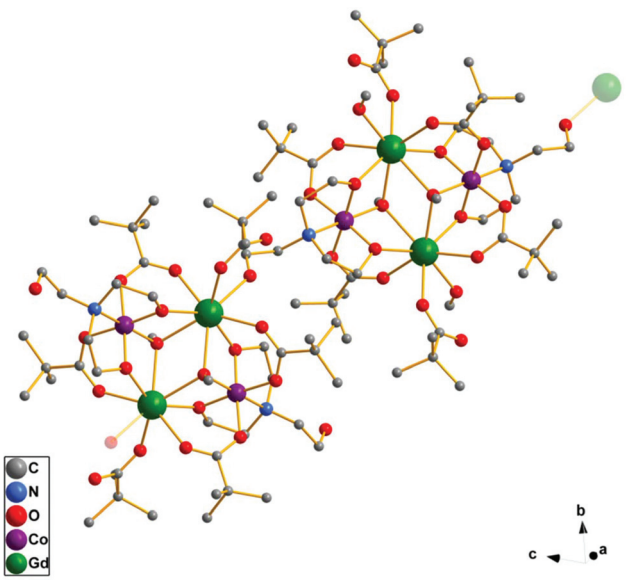

Fig. 2 Ball and sticks molecular representation of compound **6** structure, emphasizing the 1D chain arrangement. Hydrogen atoms have been omitted for the sake of clarity.

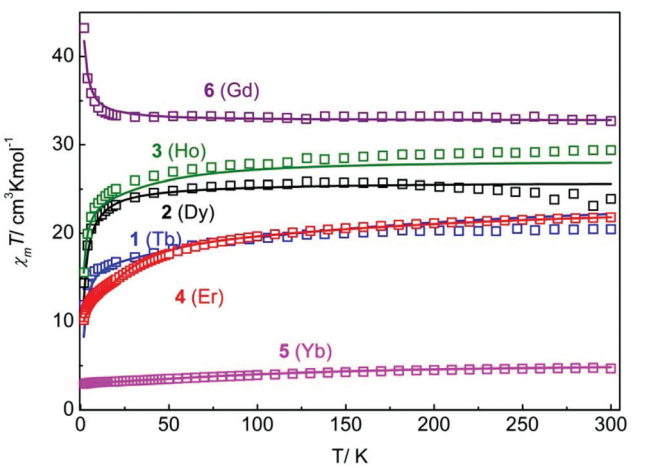

Fig. 3 $\chi_m T$ *vs.* *T* of complexes **1–6** restrained samples at 1 kOe DC magnetic field. Open squares: experimental data. Full lines: simulated, see text.

The $\chi_m T$ *vs.* T data profiles of the non-restrained samples are clearly different from the restrained sample data. The room temperature $\chi_m T$ values are manifestly above the values observed for the restrained samples suggesting the field alignment of crystallites due to magnetic moment torquing. With the exception of the Yb compound **5** (which affords identical $\chi_m T$ *vs.* T data profile to that of the restrained sample), a continuous increase of $\chi_m T$ values upon cooling is observed up to 30 K (**2** and **3**) and 50 K (**1** and **4**), where a sharp decrease is finally observed (Fig. 4). This behaviour further supports the idea of crystallite field alignment and also suggests a crystal field stabilizing higher values of m_J with respect to the lower ones.

The M *vs.* H isotherm plots at 2 K show a rapid increase in M below 10 kOe, before saturating at values of 8.5$N\beta$ (**1**), 10.6$N\beta$ (**2**), 10.6$N\beta$ (**3**), 8.6$N\beta$ (**4**) and 3.8 (**5**)$N\beta$ in the case of restrained samples (Fig. 5). The expected magnetization saturation values for two isolated Ln(III) ions are ($2g_J J$) 18$N\beta$ (**1**), 20$N\beta$ (**2**), 20$N\beta$ (**3**), 18$N\beta$ (**4**) and 8$N\beta$ (**5**). All these numbers are well above the experimental observed values, evidencing strong crystal field splitting of the different m_J components of the J ground manifold. The spin-only Gd sample (**6**) reaches a saturation value of 27.9$N\beta$, in rough agreement with four Gd(III) $S = 7/2$ sites.

On the other hand for the unrestrained samples the following saturation values are observed: 16.8$N\beta$ (**1**), 21.4$N\beta$ (**2**), 18.8$N\beta$ (**3**), 10.7$N\beta$ (**4**) and 5.2$N\beta$ (**5**) (Fig. 6). The abrupt saturation in these cases, again when comparing with restrained ones, becomes one more additional support of the field induced crystallite orientation. In agreement with susceptibility data, Yb compound **5** appears as the exception. The expected magnetization saturation value for a totally aligned sample of a single Ln(III) ion along the main quantization axis must equal $g_J m_J$ for an isolated ground m_J doublet (or pseudo-doublet in the case of integer J) state. From here, it can be

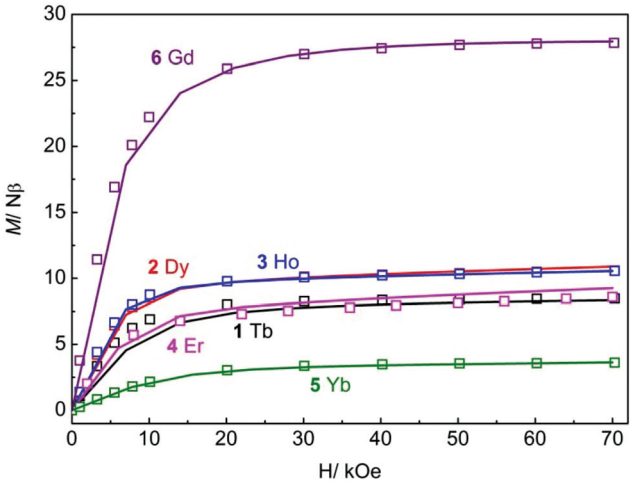

Fig. 5 *M* *vs.* *H* at 2 K of complexes **1–6** restrained samples. Open squares: experimental data. Full lines: simulated, see text.

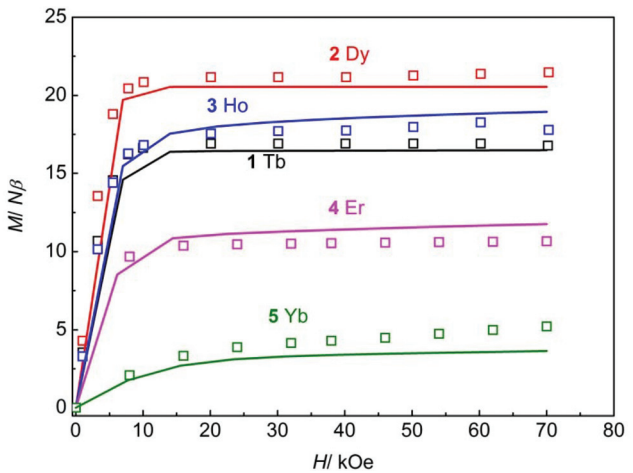

Fig. 6 *M* *vs.* H at 2 K of complexes **1–6** not-restrained samples. Open squares: experimental data. Full lines: simulated, see text.

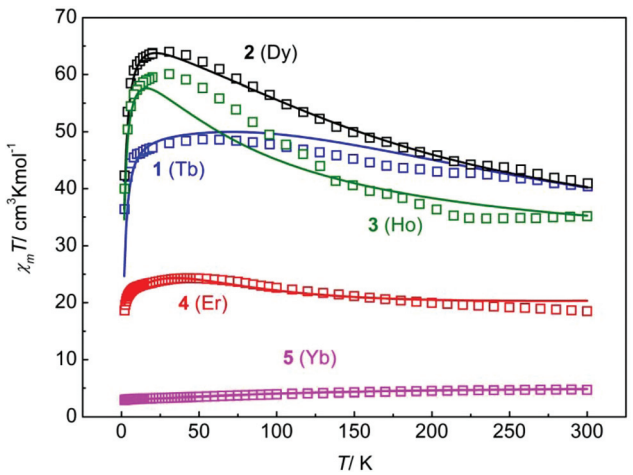

Fig. 4 $\chi_m T$ *vs.* T of complexes **1–6** not-restrained samples at 1 kOe DC magnetic field. Open squares: experimental data. Full lines: simulated, see text.

safely concluded that the crystal field stabilizes the ground state with the maximum possible m_J projection in the case of Dy compound **2**, as the expected saturation value for a completely oriented sample along the main quantization axis for $m_J = \pm 15/2$ with $g_J = 4/3$ is exactly 10$N\beta$ in close agreement with the experimental one, as two equivalent Dy(III) ions must be considered. The values observed for Tb(**1**) and Ho(**3**) are also rather close to that expected for the ground states with maximum possible m_J projection 9$N\beta \times 2$ ($g_J = 3/2$, $m_J = 6$) and 10$N\beta \times 2$ ($g_J = 5/4$, $m_J = 8$), respectively, suggesting that these are the ground doublets with possibly a very small admixture of low lying excited states. In the case of Er(**4**), the observed saturation value is well below the expected for the maximum $m_J = \pm 15/2$ with $g_J = 6/5$, 9$N\beta \times 2$, but closer to a $m_J = \pm 9/2$ (5.4$N\beta \times 2$). However, a possible admixture of other m_J values prevents anticipating the identity of the ground doublet. Finally, Yb(**5**) complex data evidence a slight increasing of

M with respect to the restrained sample data that could be tentatively ascribed to incipient crystallite alignment under higher applied magnetic fields.

In the case of compound **2**, (Dy^{III} ion; $^6H_{15/2}$, $S = 5/2$, $L = 5$, $J = 15/2$, $g_J = 4/3$) we have shown in a previous communication[12] that it is possible to account simultaneously for all the DC magnetic data (restrained and not restrained samples) behaviour through employment of a Hamiltonian for two isolated and equivalent magnetic moments $J = 15/2$ and a crystal field term expressed as Stevens equivalent operators:

$$\hat{H} = g_J \beta H(\hat{J}_1 + \hat{J}_2) + \sum_{k=2,4,6} \sum_{q=-k\ldots k} B_k^q(\hat{O}_{1k}^q + \hat{O}_{2k}^q). \quad (1)$$

Fitting the data with the PHI package[15] afforded a good agreement with experimental data employing just two CF parameters in order to avoid over-parameterization, $B_2^0 = -2.4$ cm^{-1}; $B_4^0 = 2.9 \times 10^{-3}$ cm^{-1}. It is clear that this is a minimum satisfactory set of crystal field terms, but not a complete one, as well as the Ln(III) site is not under any possible ideal symmetry. In addition, it must also be remarked that this parameter set is surely not unique and stands as a phenomenological one. In the simplest approach, the lowest temperature data can be well accounted for, by adding a HDvV exchange interaction term (which operates only on spin component of $|JM_J\rangle$ states) between both Dy(III) ions:

$$\hat{H} = g_J \beta H(\hat{J}_1 + \hat{J}_2) + \sum_{k=2,4,6} \sum_{q=-k\ldots k} B_k^q(\hat{O}_{1k}^q + \hat{O}_{2k}^q) - 2J_{exc}\hat{S}_1\hat{S}_2. \quad (2)$$

From a fitting with the optimized crystal field parameters fixed, a $J_{exc} = -0.046$ cm^{-1} value is obtained. As a further supporting data of the existence of this weak exchange interaction, Gd compound **6** data can be invoked. A simultaneous fitting of $\chi_m T$ and magnetization data for two $S = 7/2$ exchange coupled sites through a HDvV Hamiltonian affords a $J_{exc} = 0.059$ cm^{-1} ($g = 2.0$). The exchange interaction between dimeric units in the chain is expected to be vanishingly weak (*cf.* Synthesis and structural characterization) and the same J_{exc} parameter is assigned to both [$Co_2^{III}Gd_2^{III}$] moieties within the polymer repeating unit, in order to use the simplest possible model. Even when a ferromagnetic interaction is observed for compound **6**, in clear contrast to all the other members of the family, its mere existence becomes a good support for the inclusion of an exchange interaction term between Ln(III) ions.

Considering the small structural differences observed along this [$Co_2^{III}Ln_2^{III}$] family, we attempted a simultaneous data fitting of all DC magnetic data, constraining the leading B_2^0 and B_4^0 parameters to follow a tight correlation with the increasing Z number of each different Ln(III) ion to avoid over-parameterization:

$$B_k^q = A_k^q \langle r^k \rangle \alpha^k \quad (3)$$

Here the constancy of the A_k^q parameters along an isostructural Ln(III) family implies the expected correlation of B_k^q parameters with radial integrals $\langle r^k \rangle$ and hence with increasing Z ($\langle r^k \rangle$ must decrease with increasing nuclear charge) (see the ESI†).[16,17] The α^k coefficients here are the Stevens's operator equivalence factors.[17] In all cases, a fixed J_{exc} value of -0.05 cm^{-1} was included following the Hamiltonian of eqn (2), in order to avoid over-parameterization.

The finally obtained crystal field parameters are collected in Table 3. Due to the imposed constrain, the B_2^0 and B_4^0 parameters monotonously increase with increasing Z. The other parameters are most probably loosely defined but reflect, at least in a phenomenological way, the non-axial contribution to the CF and hence the degree of m_J doublets admixture for each Ln(III) ground state.

Dynamic magnetic properties

In the case of Dy compound **2**, we have previously studied possible slow relaxation of magnetization mechanisms at low temperature.[12] Alternating current (AC) magnetic susceptibility measurements show the dependence of the in-phase (χ'_m) and out-phase (χ''_m) components of the susceptibility in zero DC field. Noticeably and differing from the behaviour observed in most of the other reported [$Co_2^{III}Dy_2^{III}$] systems, two well resolved peak maxima in χ''_m were observed up to 9.5 K, Cole–Cole plots constructed between 2.5–9.5 K reveal two convoluted semicircular plots reflecting two single relaxation mechanisms with strongly differing timescales. These dynamic data can be well reproduced considering a combination of an Orbach with a quantum tunnelling mechanism for the slower process and a combination of an Orbach and Raman mechanism for the faster relaxation process. We have shown that the obtained values for the thermal barriers describing the Orbach pathways compare quite well with the low lying energy multiplets arising from the crystal field splitting parameters experimentally extracted from DC magnetic data.

Remarkably, none of the other explored members of this [$Co_2^{III}Ln_2^{III}$] family (**1–5**) evidences slow relaxation of magnetization under zero DC external field. However, after performing a field scan of the susceptibility out-of phase response (see the ESI†) at 2 K, it becomes clear that when a small external field between 1–3 kOe is applied, all of them show frequency and temperature dependent non-zero out-of phase susceptibility values, pointing to field induced SMM behaviour. Nevertheless, there are still substantial differences among them, evidencing the strong influence of the electronic structure over relaxation mechanisms in these compounds.

Only in the case of complexes **4** and **5** (Er and Yb), the AC data can be reliably analysed to extract further information about the slow relaxing processes taking place. In fact, a clear maximum can be observed in the χ''_m *vs.* T and χ''_m *vs.* frequency plots of these complexes, in contrast to Ho(**3**), where a maximum can still be recognized, and Tb(**1**) with a very weak response and no maximum available (Fig. 7 and ESI†).

These two complexes share with the Dy(**2**) compound the common feature of possessing half-integer J electronic ground state values. It is accepted that non-Kramers electronic ground states of Ln(III) systems exhibit zero-field fast quantum

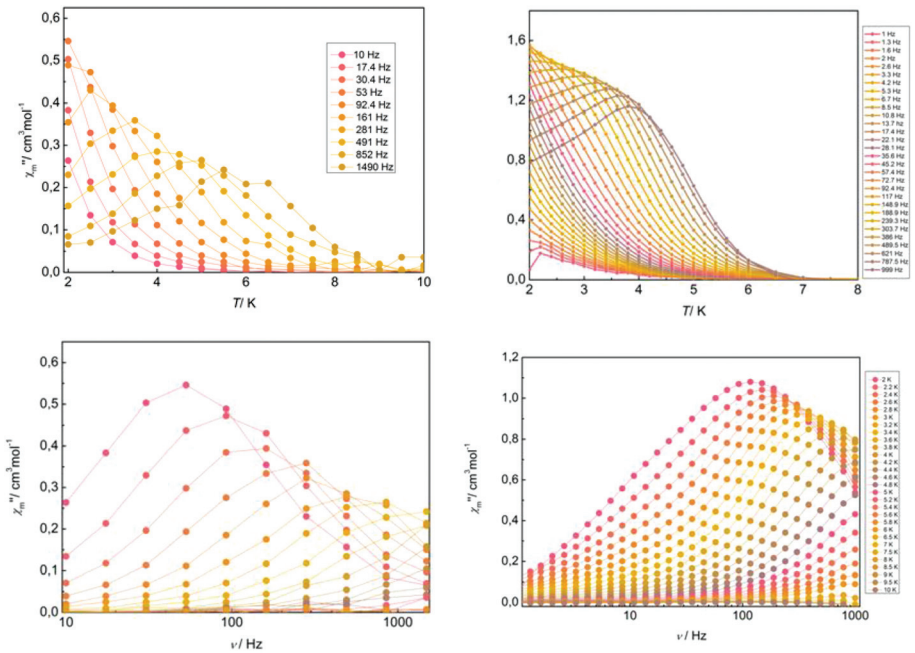

Fig. 7 Temperature (top) and frequency (bottom) AC out of phase susceptibility data dependence of complexes **4**, Er (right) and **5**, Yb (left) under 1.5 kOe DC applied field. Full lines are just for guiding the eye. Frequency dependence plot is shown in logarithmic scale.

tunnelling relaxation processes due to admixing of m_J states in contrast to Kramers ground doublets.[7a] This is in full agreement with the weak and low temperature shifted out-of-phase susceptibility signal observed for complexes **1** (Tb, $J = 6$) and **3** (Ho, $J = 8$).

Fitting of Cole–Cole plots (Fig. 8) through a generalized Debye model (following the same procedure for the previously reported Dy compound **2** [12]) for complexes **4** and **5** under external applied fields of 1500 Oe allowed extracting relaxation times within the temperature range of 2–6 K, with α values between 0.06–0.34. In the case of Er compound **4**, two clear distinct relaxation processes were found, one of them essentially temperature independent, possibly ascribable to a thermal assisted quantum tunnelling relaxation path. Temperature dependence of these characteristic relaxation times can be further analysed in terms of the following general equation:[17]

$$\frac{1}{\tau} = C_{\mathrm{Raman}} T^{n} + \frac{1}{\tau_{\mathrm{QT}}} + \frac{1}{\tau_0} \exp\left(-\frac{U_{\mathrm{eff}}}{kT}\right). \qquad (4)$$

Here the exponential term corresponds to the Orbach mechanism, distinctive due to its thermal barrier parameter and recognized through a linear $\ln \tau$ *vs.* T^{-1} plot. When looking at the $\ln \tau$ *vs.* T^{-1} plots (Fig. 8), a linear regime is readily identified in the high temperature data in the case of complex **5**, while in the case of compound **4**, there is no evident linear regime in the whole temperature range. These observations suggest that an Orbach mechanism is operative in the case of the Yb complex but not in the case of the Er analogue.

In fact, the best fitting parameters obtained after exploring all different contributions of eqn (4) are: $C_{\mathrm{Raman}} = 3.5 \times 10^{-2}$ $\mathrm{s^{-1}\ K^{-7}}$ ($n = 7$) and $\tau_{\mathrm{QT}} = 5.1 \times 10^{-3}$ s (**5**); $U_{\mathrm{eff}} = 23\ \mathrm{cm^{-1}}$, $\tau_0 = 2.1 \times 10^{-6}$ s and $\tau_{\mathrm{QT}} = 1.3 \times 10^{-2}$ s (**4**).

Regarding the Ho(**3**) complex, reliable Cole–Cole data fitting was not possible, but from the maximum in the χ'' *vs.* T data profile and its frequency dependency, it is still possible to extract dynamic information. In fact a rough linear regime following an Orbach mechanism is observed with parameters: $U_{\mathrm{eff}} = 30\ \mathrm{cm^{-1}}$, $\tau_0 = 6.2 \times 10^{-9}$ (see the ESI†).

As found for the Dy(**2**) compound, in the case of the Yb(**5**) compound, the Orbach thermal barrier found from AC data is in rough agreement with crystal field energy level splitting as arising from DC data, which offers a thermal barrier from the ground doublet ($|\pm1/2\rangle$(49%);$|\pm3/2\rangle$(31%);$|\pm5/2\rangle$(12%)) to the first excited doublet ($|\pm1/2\rangle$(39%);$|\pm3/2\rangle$(38%);$|\pm5/2\rangle$(18%)) of *ca.* 12 $\mathrm{cm^{-1}}$ (see the ESI†). The predominance of the lowest m_J doublet in the ground state may explain the lack of crystallite orientation observed in this complex in clear contrast to all other explored analogues.

The same agreement applies for the Ho(**3**) compound where the energy difference between the ground doublet ($|\pm8\rangle$(90%);$|\pm4\rangle$(10%)) and the first excited doublet ($|\pm4\rangle$(80%);$|\pm8\rangle$(10%);$|0\rangle$(9%)) as arising from crystal field parameters is *ca.* 35 $\mathrm{cm^{-1}}$ (see the ESI†).

In the case of the Er(**5**) complex, the absence of an Orbach mechanism precludes comparison with crystal field energy level splitting; nevertheless an extensive admixture of doublets can be recognized (see the ESI†).

A summary of magnetization relaxation dynamics for the whole $[Co^{III}_2Ln^{III}_2]$ family is shown in Table 4.

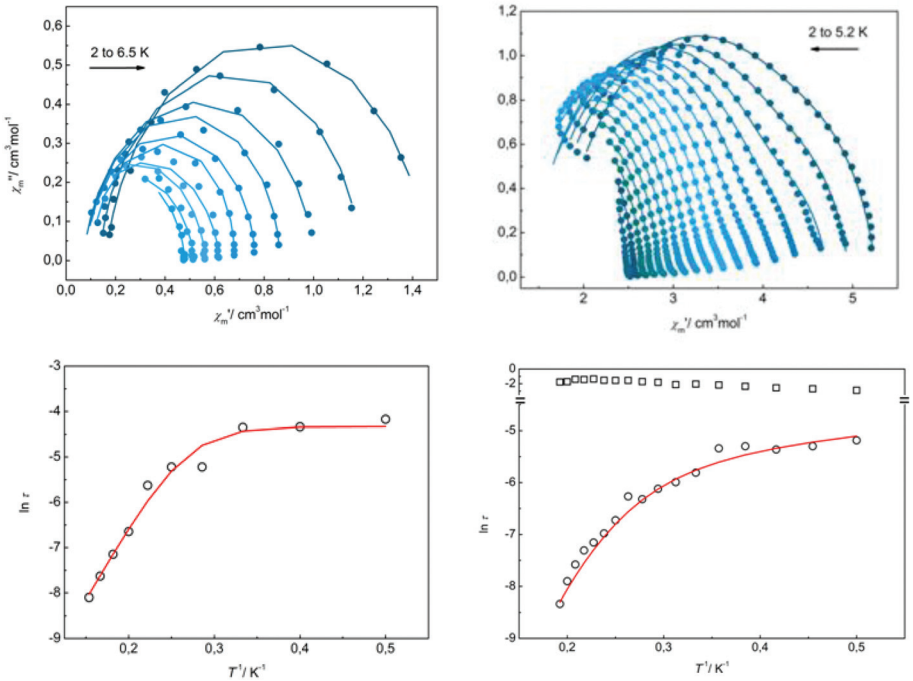

Fig. 8 Top: Cole–Cole plot of AC data at 1.5 kOe external applied field of complexes **4**, Er (right) and **5**, Yb (left). Full lines are best fitting to a generalized Debye model, see text. Bottom: Temperature dependence of characteristic magnetization relaxation times as ln *t vs.* T^{-1} plots of complexes **4**, Er (right) and **5**, Yb (left). Full line: best fitting plot, see text. Squares: temperature independent relaxation process.

Conclusions

We have successfully prepared and structurally characterized a family of butterfly-like $[Co_2^{III}Ln_2^{III}]$ complexes where all magnetic properties are due to the Ln(III) ions. All of them proved to be iso-structural with the exception of the Gd(III) one which is a one dimensional chain. This structural rigidity together with the high tendency of free crystallites to align under an applied magnetic field allowed an overall DC magnetic data treatment to extract in a phenomenological way crystal field parameters and hence ground state multiplet energy level splitting. The Dy(III) member is the only one showing slow relaxation of magnetization under zero DC applied field, while all the others need a small DC applied field. This observation correlates with the strong axial crystal field environment found for the Dy(III) complex when compared with the other members of this family. Fast tunnelling mechanisms can be inferred in the case of the Ln(III) complexes baring integer *J* ground state multiplets, namely Tb and Ho, which evidence the lowest blocking temperatures in AC susceptibility experiments.

In summary, with the aid of field aligned sample DC magnetic measurements and molecular structure invariance we have been able to obtain a rather convincing picture of ground *J* manifold crystal field splitting of the different Ln(III) members of the family, showing good agreement with dynamic data as arising from AC susceptibility measurements. This is a key point when dealing with these molecular nanomagnet systems as it can contribute in the rationalization of the link between the electronic structure and magnetization reversal thermal barrier. We remarked however that this simplified phenomenological approach must be validated through spectroscopic techniques which can locally probe the *J* manifold level splitting. We are currently exploring different alternatives to tackle this issue.

Experimental section

Material and physical measurements

$[Co_2(\mu\text{-}OH_2)(\mu\text{-}Piv)_2(Piv)_2(HPiv)_4]$, Piv = trimethylacetate, was prepared following a previously reported procedure.[18] All other chemicals were reagent grade and used as received without further purification. Elemental analysis for C, H and N was performed with a Carlo Erba 1108 analyzer.

Synthesis of complexes

Synthesis of Co_2Ln_2 $(OMe)_2(teaH)_2(Piv)_6$, Ln = Tb(1), Dy(2), Ho(3), Er(4), Yb(5). $Co_2(OH_2)(Piv)_4(HPiv)_4$ (100 mg, 0.1 mmol) and $Ln(NO_3)_3{\cdot}xH_2O$ (54 mg, ~0.15 mmol) were dissolved in 10 mL of MeCN, followed by the addition of triethanolamine (60 mg, 0.4 mmol) and triethylamine (61 mg, 0.6 mmol) dissolved in 10 ml of acetonitrile, affording a purple solution. The latter was then stirred for an hour, filtered and allowed to stand sealed at room temperature. Within 3–4 weeks a crop of blue needles appeared. This product was filtered and redissolved in a 1 : 1 MeCN/MeOH mixture. After a couple of days blue blocks of the final product had crystallized with averaged yields of 48%, *ca.* 25 mg.

Anal. Calcd (found) for $C_{44}H_{86}Co_2Ln_2N_2O_{20}$ C, 37.8 (37.8); H, 6.2 (6.2); N, 2.0 (1.9) (**1**); C, 37.6 (37.2); H, 6.2 (5.5); N, 2.0 (2.1) (**2**); C, 37.5 (37.4); H, 6.2 (6.1); N, 2.0 (2.2) (**3**); C, 37.3 (37.4); H, 6.1 (6.1); N, 2.0 (2.0) (**4**); C, 37.0 (37.1); H, 6.1 (5.9); N, 2.0 (2.1) (**5**).

Synthesis of $[Co_2^{III}Gd_2^{III}(OCH_3)_2(OHCH_3)_2(tea)_2(Piv)_4(HPiv)_2][Co_2^{III}Gd_2^{III}(OCH_3)_2(tea)_2(Piv)_4(HPiv)_2]_n$ (6). $Co_2(OH_2)(Piv)_4(HPiv)_4$ (100 mg, 0.1 mmol) and $Gd(NO_3)_3{\cdot}xH_2O$ (65.8 mg, ~0.15 mmol) were dissolved in 10 mL of MeCN, followed by the addition of triethanolamine (60 mg, 0.4 mmol) and triethylamine (61 mg, 0.6 mmol) dissolved in 10 ml of acetonitrile, affording a purple solution. The latter was then stirred for an hour, filtered and allowed to stand sealed at room temperature. Within 3–4 weeks a crop of blue needles appeared. This product was filtered and re-dissolved in a 1 : 1 MeCN/MeOH mixture. After a couple of days blue blocks of the final product had crystallized with a yield of 16%, *ca.* 36 mg.

Anal. Calcd (found) for $C_{90}H_{180}Co_4Gd_4N_4O_4$: C, 37.9 (37.2); H, 6.3 (5.5); N, 2.0 (2.1).

Magnetic measurements

Magnetic measurements were performed with a Quantum Design MPMS XL-7 SQUID magnetometer. All experimental magnetic data were corrected for the diamagnetism of the sample holders and of the constituent atoms (Pascal's tables). DC measurements were conducted from 2 to 300 K at 1 kOe and at 2 K in the range 1–70 kOe. AC measurements were performed at driving frequencies ranging from 10 to 1500 Hz with an AC field amplitude of 3 Oe in zero DC field and under small applied DC fields. In the samples where free movement of crystallites was prevented, silicone grease was employed for embedding. When silicone is not used, the sample completely aligned with the field quantization axis as evidenced by the magnetization saturation values achieved.

Magnetic data fitting

We employed the PHI package that allows the simultaneous fit of susceptibility and magnetization data. In order to attempt the simultaneous data fitting of the restrained and not-restrained susceptibility and magnetization data of complexes **1–5**, by means of crystal field parameters we proceeded as follows: we started the fitting of data for each Ln(III) from different initial parameters, iteratively between restrained and not-restrained data until convergence of both parameter sets in a unique one. We started employing only B_2^0 and B_4^0 CF parameters, and subsequently added more parameters only if convergence cannot be achieved. We further refined this procedure by imposing limits to the B_2^0 and B_4^0 CF parameters to force them entering an almost linear progression with Ln(III) *f* electron counting (increasing one unit in *Z*) until new convergence was reached.

Table 1 Crystallographic data for **1–3**

	1	**2**	**3**
Empirical formula	$C_{44}H_{86}Co_2Tb_2N_2O_{20}$	$C_{44}H_{86}Co_2Dy_2N_2O_{20}$	$C_{44}H_{86}Co_2Ho_2N_2O_{20}$
Formula weight	1398.84	1406.01	1410.86
T (K)	298 (2)	298 (2)	298 (2)
Crystal system	Triclinic	Triclinic	Triclinic
Space group	$P\bar{1}$	$P\bar{1}$	$P\bar{1}$
a (Å)	10.9445(15)	10.9410(4)	10.9560(5)
b (Å)	11.2284(15)	11.2485(4)	11.2392(4)
c (Å)	12.2089(16)	12.2043(5)	12.1874(4)
α (°)	104.544(11)	104.787(3)	104.953(3)
β (°)	90.934(11)	90.745(3)	90.779(3)
γ (°)	94.486(11)	94.220(3)	93.973(3)
V (Å^3)	1446.8(3)	1447.50(9)	1445.65(9)
Z	1	1	1
D_{calc} (mg m^{-3})	1.605	1.613	1.621
Absorption coefficient (mm^{-1})	3.046	3.183	3.339
F(000)	708	710	712
λ (Å)	0.71073	0.71073	0.71073
θ range data collection (°)	3.72–26.99	3.71–27.0	3.73–27.0
Index ranges	$-13 \le h \le 13$ $-14 \le k \le 14$ $-15 \le l \le 15$	$-13 \le h \le 13$ $-14 \le k \le 14$ $-15 \le l \le 15$	$-13 \le h \le 13$ $-14 \le k \le 14$ $-15 \le l \le 15$
Reflections collected/unique	15 511/6223	18 734/6252	15 670/6221
R_{int}	0.0424	0.0550	0.0488
Observed reflections [$I > 2\sigma(I)$]	5471	5086	4986
Completeness (%)	99.7	99.1	99.7
Maximum/minimum transmission	1.0000/0.7431	1.000/0.544	1.0000/0.9532
Data/restraints/parameters	6223/9/344	6252/30/314	6221/9/343
Goodness-of-fit (GOF) on F^2	1.000	1.076	1.027
Final R-index [$I > 2\sigma(I)$]/all data	0.0304/0.0376	0.0384/0.0557	0.0391/0.0586
wR index [$I > 2\sigma(I)$]/all data	0.0701/0.0746	0.0878/0.1011	0.0799/0.0934
Largest peak and hole (e A^{-3})	−0.850 and 0.715	1.399 and −1.029	1.307 and −0.966
Weights, w	$1/[\sigma^2(F_o^2) + (0.0333P)^2 + 1.0819P]$ where $P = (F_o^2 + 2F_c^2)/3$	$1/[\sigma^2(F_o^2) + (0.0423P)^2 + 1.4130P]$ where $P = (Fo^2 + 2F_c^2)/3$	$1/[\sigma^2(F_o^2) + (0.0324P)^2 + 2.3610P]$ where $P = (F_o^2 + 2F_c^2)/3$

Table 2 Crystallographic data for **4–6**

	4	**5**	**6**
Empirical formula	$C_{44}H_{86}Co_2Er_2N_2O_{20}$	$C_{44}H_{86}Co_2Yb_2N_2O_{20}$	$C_{45}H_{90}Co_2Gd_2N_2O_{21}$
Formula weight	1415.52	1427.08	1427.54
T (K)	170(2)	298(2)	298(2)
Crystal system	Triclinic	Triclinic	Triclinic
Space group	$P\bar{1}$	$P\bar{1}$	$P\bar{1}$
a (Å)	10.9196(9)	10.9901(6)	10.3082(10)
b (Å)	11.1887(5)	11.2049(5)	15.7274(13)
c (Å)	12.1589(10)	12.1420(4)	20.7623(18)
α (°)	105.292(6)	105.440(3)	76.602(7)
β (°)	90.692(7)	90.945(4)	80.498(7)
γ (°)	93.941(5)	93.375(4)	76.496(8)
V (Å^3)	1428.84(18)	1437.94(11)	3161.9(5)
Z	1	1	2
D_{calc} (mg m^{-3})	1.645	1.648	1.499
Absorption coefficient (mm^{-1})	3.546	3.858	2.651
F(000)	714	718	1448
λ (Å)	0.71073	0.71073	0.71073
θ range data collection (°)	3.49–27.0	3.72–27.0	3.58–27.0
Index ranges	$-13 \le h \le 13$ $-14 \le k \le 14$ $-15 \le l \le 15$	$-13 \le h \le 13$ $-14 \le k \le 14$ $-15 \le l \le 15$	$-13 \le h \le 12$ $-19 \le k \le 19$ $-26 \le l \le 26$
Reflections collected/unique	24 188/6209	18 209/6196	39 632/13 655
R_{int}	0.0416	0.0409	0.0561
Observed reflections [$I > 2\sigma(I)$]	5561	5605	10 291
Completeness (%)	99.5	99.7	99.7
Maximum/minimum transmission	1.000/0.935	1.000/0.474	1.000/0.657
Data/restraints/parameters	6209/15/344	6196/9/344	13 655/905/802
Goodness-of-fit (GOF) on F^2	1.056	1.054	1.077
Final R-index [$I > 2\sigma(I)$]/all data	0.0265/0.0326	0.0279/0.0336	0.0379/0.0600
wR index [$I > 2\sigma(I)$]/all data	0.0605/0.0644	0.0638/0.0692	0.0780/0.0923
Largest peak and hole (e A^{-3})	0.617 and −0.626	0.780 and −0.758	1.221 and −0.637
Weights, w	$1/[\sigma^2(F_o^2) + (0.0262P)^2 + 1.0385P]$ where $P = (F_o^2 + 2F_c^2)/3$	$1/[\sigma^2(F_o^2) + (0.0307P)^2 + 0.6483P]$ where $P = (F_o^2 + 2F_c^2)/3$	$1/[\sigma^2(F_o^2) + (0.0297P)^2 + 0.1144P]$ where $P = (F_o^2 + 2F_c^2)/3$

Table 3 Best fitting crystal field parameters (cm^{-1}) of complexes **1–5**[a]

	B_0^2	B_0^4	B_0^6	B_2^4	B_4^4	B_4^6
1 Tb	−3.9	-2.0×10^{-2}	—	—	−0.17	-4.7×10^{-3}
2 Dy	−2.4	2.9×10^{-3}	—	—	—	—
3 Ho	−0.8	1.5×10^{-3}	-1.0×10^{-4}	—	$\pm2.7 \times 10^{-2}$	$\pm7.5 \times 10^{-6}$
4 Er	0.9	1.9×10^{-3}	-7.0×10^{-5}	$\pm9.2 \times 10^{-2}$	1.7×10^{-2}	-6.7×10^{-4}
5 Yb	9.7	6.0×10^{-2}	—	$\pm5.7 \times 10^{-2}$		±0.13

[a] Uncertainties in the parameters (confidence interval up to 95%) range from less than 5% for the axial components up to 15% for the non-axial ones.

Table 4 Magnetization dynamics data of complexes [$Co^{III}_2Ln^{III}_2$]

Ln	Mechanism	Parameters
2 Dy[a]	Orbach	$\tau_0 = 6.1 \times 10^{-7}$ s; $U_{eff} = 35$ cm^{-1}; $\tau_{QT} = 7.3$ s
	Orbach + Raman	$\tau_0 = 1.2 \times 10^{-9}$ s; $U_{eff} = 88$ cm^{-1}
3 Ho[b]	Orbach	$\tau_0 = 6.2 \times 10^{-9}$ s; $U_{eff} = 30$ cm^{-1}
4 Er[c]	Raman	$\tau^1_{QT} = 5.1 \times 10^{-3}$ s; $C_{Ram} = 3.5 \times 10^{-2}$ s^{-1} K^{-7} ($n = 7$); $\tau^2_{QT} = 0.103$ s
5 Yb[c]	Orbach	$\tau_0 = 2.1 \times 10^{-6}$ s; $U_{eff} = 23$ cm^{-1}; $\tau_{QT} = 1.3 \times 10^{-2}$ s

[a] Ref. 12, 0 DC external field. [b] 1.5 kOe external DC field. [c] 3 kOe external DC field.

X-ray structure determination

Crystal structures of compounds **1–6** (with the exception of compound **2** previously reported) were determined with an Oxford Xcalibur, Eos, Gemini CCD area-detector diffractometer using graphite-monochromated Mo-Kα radiation (λ = 0.71069 Å) at 298 K (170 K in the case of complex **4**). Data were corrected for absorption with CrysAlisPro, Oxford Diffraction

Ltd, Version 1.171.33.66, applying an empirical absorption correction using spherical harmonics, implemented in the SCALE3 ABSPACK scaling algorithm.[19] The structure was solved by direct methods with SIR97[20] and refined with full-matrix least-squares on F^2 with SHELXL-2014[21] under the WinGX platform.[22] Hydrogen atoms were added geometrically and refined as riding atoms with a uniform value of U_{iso}. In structures **1**, **3**, **4** and **5** two pivalate methyl groups; one carbon atom and one oxygen atom from an ethanol fragment of the triethanolamine ligand, were found disordered around two positions and split refined with free occupancy factors. In structure **6** five pivalate methyl groups were found to be disordered around two positions and split refined with free occupancy factors. The final crystallographic data and values of R_1 and wR are listed in Tables 1 and 2 while the main angles and distances are listed in the ESI.† CCDC 1489634–1489638 contain the supplementary crystallographic data for this paper.

Acknowledgements

We gratefully acknowledge UBA, ANPCYT and CONICET for funding resources. PA is a staff member of CONICET and AVF is a doctoral fellow of CONICET.

References

1 M. Affronte and F. Troiani, in *Mol. Magnets Phys. Appl*, ed. J. Bartolome, J. Luis and F. Fernandez, Springer-Verlag, Heidelberg, 2014, pp. 249–273.
2 Y.-Z. Zheng, G.-J. Zhou, Z. Zheng and R. E. P. Winpenny, *Chem. Soc. Rev.*, 2014, **43**, 1462.
3 S. Sanvito, *Chem. Soc. Rev.*, 2011, **40**, 3336.
4 D. Gatteschi, R. Sessoli and J. Villain, *Molecular Nanomagnets*, Oxford University Press, 2006.
5 (*a*) G. A. Craig and M. Murrie, *Chem. Soc. Rev.*, 2015, **44**, 2135; (*b*) H. L. C. Feltham and S. Brooker, *Coord. Chem. Rev.*, 2014, **276**, 1.
6 G. Aromí and E. K. Brechin, in *Single-Molecule Magnets Relat. Phenom.*, ed. R. Winpenny, 2006, pp. 1–67.
7 (*a*) S. T. Liddle and J. van Slageren, *Chem. Soc. Rev.*, 2015, **44**, 6655; (*b*) J. D. Rinehart and J. R. Long, *Chem. Sci.*, 2011, **2**, 2078.
8 D. N. Woodruff, R. E. P. Winpenny and R. A. Layfield, *Chem. Rev.*, 2013, **113**, 5110.
9 K. Liu, W. Shi and P. Cheng, *Coord. Chem. Rev.*, 2015, **289–290**, 74.
10 (*a*) S. K. Langley, C. M. Forsyth, B. Moubaraki and K. S. Murray, *Dalton Trans.*, 2015, **44**, 912; (*b*) S. K. Langley, D. P. Wielechowski, V. Vieru, N. F. Chilton, B. Moubaraki, L. F. Chibotaru and K. S. Murray, *Chem. Sci.*, 2014, **5**, 3246; (*c*) S. K. Langley, D. P. Wielechowski, V. Vieru, N. F. Chilton, B. Moubaraki, B. F. Abrahams, L. F. Chibotaru and K. S. Murray, *Angew. Chem., Int. Ed.*, 2013, **52**, 12014.
11 (*a*) S. K. Langley, C. Le, L. Ungur, B. Moubaraki, B. F. Abrahams, L. F. Chibotaru and K. S. Murray, *Inorg. Chem.*, 2015, **54**, 3631; (*b*) S. K. Langley, N. F. Chilton, B. Moubaraki and K. S. Murray, *Inorg. Chem. Front.*, 2015, **2**, 867; (*c*) S. K. Langley, L. Ungur, N. F. Chilton, B. Moubaraki, L. F. Chibotaru and K. S. Murray, *Inorg. Chem.*, 2014, **53**, 4303; (*d*) S. K. Langley, N. F. Chilton, B. Moubaraki and K. S. Murray, *Inorg. Chem.*, 2013, **52**, 7183; (*e*) S. K. Langley, N. F. Chilton, B. Moubaraki and K. S. Murray, *Chem. Commun.*, 2013, **49**, 6965; (*f*) S. K. Langley, N. F. Chilton, L. Ungur, B. Moubaraki, L. F. Chibotaru and K. S. Murray, *Inorg. Chem.*, 2012, **51**, 11873.
12 A. V. Funes, L. Carrella, E. Rentschler and P. Alborés, *Dalton Trans.*, 2014, **43**, 2361.
13 (*a*) A. V. Funes, L. Carrella, L. Sorace, E. Rentschler and P. Alborés, *Dalton Trans.*, 2015, **44**, 2390; (*b*) I. C. Lazzarini, A. V. Funes, L. Carrella, L. Sorace, E. Rentschler and P. Alborés, *Eur. J. Inorg. Chem.*, 2014, **2014**, 2561; (*c*) I. C. Lazzarini, L. Carrella, E. Rentschler and P. Alborés, *Polyhedron*, 2012, **31**, 779; (*d*) P. Alborés and E. Rentschler, *Angew. Chem., Int. Ed.*, 2009, **48**, 9366.
14 S. Alvarez, P. Alemany, D. Casanova, J. Cirera, M. Llunell and D. Avnir, *Coord. Chem. Rev.*, 2005, **249**, 1693.
15 N. F. Chilton, R. P. Anderson, L. D. Turner, A. Soncini and K. S. Murray, *J. Comput. Chem.*, 2013, **34**, 1164.
16 N. Ishikawa, *J. Phys. Chem. A*, 2003, **107**, 5831.
17 A. Abraham and B. Bleaney, *Electron Paramagnetic Resonance of Transition Ions*, Oxford University Press, 1970.
18 G. Aromí, A. S. Batsanov, P. Christian, M. Helliwell, A. Parkin, S. Parsons, A. A. Smith, G. A. Timco and R. E. P. Winpenny, *Chem. – Eur. J.*, 2003, **9**, 5142.
19 *SCALE3 ABSPACK: Empirical absorption correction, CrysAlis – Software package*, Oxford Diffraction Ltd, Oxford, 2006.
20 A. Altomare, M. C. Burla, M. Camalli, G. L. Cascarano, C. Giacovazzo, A. Guagliardi, A. G. G. Moliterni, G. Polidori and R. Spagna, *J. Appl. Crystallogr.*, 1999, **32**, 115.
21 G. M. Sheldrick, *Acta Crystallogr., Sect. A: Fundam. Crystallogr.*, 2008, **64**, 112.
22 L. J. Farrugia, *J. Appl. Crystallogr.*, 2012, **45**, 849.